Statistics of polymer adsorption under shear flow

Gui-Li He,[a] René Messina, and Hartmut Löwen
Institut für Theoretische Physik II, Heinrich-Heine-Universität Düsseldorf, Universitätsstrasse 1, D-40225 Düsseldorf, Germany

(Received 2 October 2009; accepted 23 February 2010; published online 29 March 2010)

Using nonequilibrium Brownian dynamics computer simulations, we have investigated the steady state statistics of a polymer chain under three different shear environments: (i) linear shear flow in the bulk (no interfaces), (ii) shear vorticity normal to the adsorbing interface, and (iii) shear gradient normal to the adsorbing interface. The statistical distribution of the chain end-to-end distance and its orientational angles are calculated within our computer simulations. Over a wide range of shear rates, this distribution can be mapped onto a simple theoretical finite-extensible-nonlinear-elastic dumbbell model with fitted anisotropic effective spring constants. The tails of the angular distribution functions are consistent with scaling predictions borrowed from the bulk dumbbell model. Finally, the frequency of the characteristic periodic tumbling motion has been investigated by simulation as well and was found to be sublinear with the shear rate for the three setups, which extends earlier results done in experiments and simulations for free and tethered polymer molecules without adsorption. © *2010 American Institute of Physics*. [doi:10.1063/1.3361673]

I. INTRODUCTION

Adsorption of macromolecules in flowing fluids arises in countless practical or potential applications. For instance the process of implanting biotissues happens in the shear flow field of the blood stream and represents a key challenge[1] in the cure of disabilities due to malfunctioning organs. In gene therapy, the transport of DNA to a desired target site is another big challenge.[2] The control of proteins changing their biofunctionality during adsorption to surfaces[3] is also a quite interesting topic for biotechnical application. Furthermore, the influence of adsorption under flow is important in microfluidic devices.[4] For example, shear flow generates stretched polymer chains which can be used for microcircuit construction from single molecules.[5,6]

Experimentally, polymers under shear flow have been investigated for many decades.[7–18] Due to both an elongational and a rotational components stemming from the flow inhomogeneity, the dynamics or statistics of sheared molecules is complex. Tumbling motion was recently addressed experimentally in the bulk[19–21] but not for adsorbed polymers.

On the theoretical side, Hinch[22] has developed a theory for a continuous flexible string under shear flow and also examined the effect of weak Brownian motion on the polymer.[23] Recently, analyzing the statistics of the chain end-to-end extension and orientation, Chertkov and co-workers[24] have addressed the polymer tumbling motion under shear flow. Furthermore, Winkler[25] has analytically studied the dynamics of semiflexible polymers under the influence of shear flow. Numerical studies based on a simple polymer *dumbbell* in linear shear flows have been carried out to analyze the cyclic motion by Celani *et al.*[26] and Puliafito *et al.*[27]

Computer simulations have also been employed to study polymers under shear flow. Chopra and Larson[28] performed Brownian dynamics (BD) for polymer chains that are either irreversibly adsorbing or nonadsorbing. Later, Panwar and Kumar[29] successfully extended this work to polyelectrolyte chains. None of these studies took polymer-wall hydrodynamic interaction (HI) into account. The effect of the HI on the adsorption process can be important, as shown in the work of Hoda and Kumar.[30–32] First, using a bead-spring dumbbell model, they analytically developed a kinetic theory which predicts a competition between bead-wall HI and bead-wall attraction.[30] As a result, a desorption due to the dominance of HI at a high enough shear rate takes place.[30] Then using BD simulations with HI, they confirmed their former predictions[30] and developed a scaling law for a critical shear rate at which chains desorb.[31] Later they generalized their work by incorporating the effects of solvent quality and charge patterning.[32] In the literatures, there also exist simulation data about the tumbling motion for free chains[19,33,34] and end-tethered polymers[35,36] and confined polymers in microchannels.[37]

Although the statistics of the polymer end-to-end extension and angular orientation have been investigated experimentally and theoretically in the past, most of the relative work is essentially focused on the bulk case. In this paper, our main goal is to address these properties for an *adsorbed* polymer chain under linear shear flow. For a pulled adsorbed chain, a simulation study was recently performed in Ref. 38. The problem of the adsorbed case is more complex than in the bulk since adsorption will interfere and compete with tumbling motion in the shear flow. Moreover, the chain conformational behavior will depend on the direction of the shear flow relative to the adsorbing substrate. For a planar adsorbing interface, there are two basic possibilities for the shear flow direction: the shear gradient can be directed either perpendicular or parallel to the adsorbing interface.

In this work, we consider these two cases in conjunction

[a]Electronic mail: guili@thphy.uni-duesseldorf.de.

with the bulk system as a reference and calculate the probability distribution function (PDF) of the chain extension by using BD computer simulations. We find that the PDF of the polymer chain extension can be mapped by a simple theoretical finite-extensible-nonlinear-elastic (FENE) dumbbell model via two fit parameters, namely, an effective shear rate and an effective spring constant. The tails of the angular PDFs obtained by the simulations are in good agreement with theoretical predictions stemming from the bulk. Surprisingly, they fit even better than in the bulk for a wide shear rate regime when the shear gradient is directed parallel to the adsorbing interface. For the situation where the shear gradient is perpendicular to the interface, disturbances of the bulk fluctuations due to interface adsorption lead to significant deviations from a simple dumbbell model. We also explore the inner bond-bond angles (BBAs) of the chain and the frequency of the characteristic periodic tumbling motion which was found to be sublinear with the shear rate. This extends earlier experimental and simulation studies for free and tethered polymer molecules without adsorption.

The outline of this article is as follows: Sec. II describes the details of the simulation model. Section III contains the results in which Sec III A deals with the statistics of the chain extension; Sec. III B shows the angular degrees of freedom (for in-adsorption-plane and off-adsorption-plane orientations, respectively); Sec. III C is discussing the shear rate dependency of the bond-bond angle; and the last part Sec. III D is devoted to analysis of the tumbling motion frequency. Finally, a summary of our work is presented and discussed in Sec. IV.

II. THE MODEL

This section provides details about our polymer chain model employed in nonequilibrium BD computer simulations.[39,40] The macromolecular chain is modeled as a sequence of $N=48$ coarse-grained spring-beads. The beads are labeled $i=0,1,2,\ldots,N-1$. Thereby, the equation of motion of the ith bead located at a position $\mathbf{r}_i(t)=(x_i(t),y_i(t),z_i(t))$ at time t is given by the finite integration scheme

$$\mathbf{r}_i(t+\delta t)=\mathbf{r}_i(t)+\frac{D_0}{k_BT}\mathbf{F}_i\delta t+\delta\mathbf{G}_i+\dot{\gamma}q_i(t)\delta t\mathbf{e}_x, \tag{1}$$

where $\mathbf{r}_i(t+\delta t)$ is the updated bead position at a later time $t+\delta t$. We now explain in details all the constitutive terms of Eq. (1). D_0, k_B, and T stand for the free diffusion constant, Boltzmann's constant, and the absolute temperature, respectively. The vector $\mathbf{F}_i$ is the total conservative force that will be fully described later. $\delta\mathbf{G}_i$ is the Gaussian stochastic displacement with 0 mean and variance $2D_0\delta t$ for each Cartesian component. The last term in Eq. (1) stems from the contribution of the shear flow being in the x-direction, with $\mathbf{e}_x$ denoting the corresponding unit vector and $\dot{\gamma}$ the shear rate. $q_i(t)$ in Eq. (1) can be either $y_i(t)$ or $z_i(t)$ depending on the chosen shear gradient direction. More precisely: (i) $q_i(t)=y_i(t)$ refers to a normal vorticity (NV) direction perpendicular to the adsorbing interface, as sketched in Fig. 1(a); (ii) $q_i(t)=z_i(t)$ corresponds to a normal gradient (NG), see Fig. 1(b). In other words, the shear gradient is in-plane with the adsorbing interface for the NV case whereas it becomes off-plane for the NG case.[41] Realizing the NV case is more challenging, but in principle possible if the polymer is not on a solid substrate but confined to a fluid-gas interface. Then there can be a shear flow within the interface which is not possible at a solid wall.[42] The aforementioned conservative force $\mathbf{F}_i$ has three contributions:

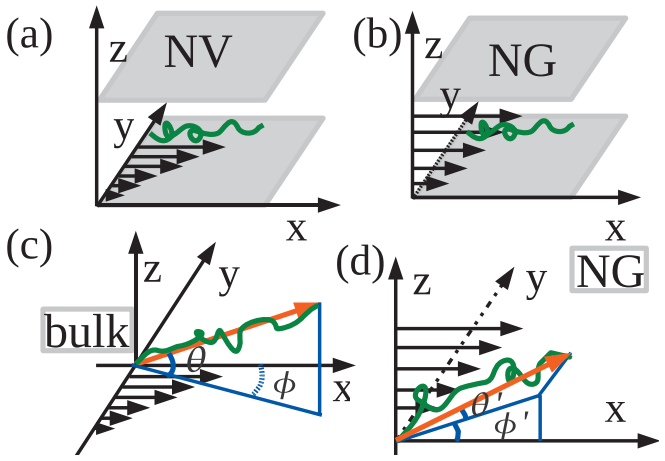

FIG. 1. Sketches of simulation model: (a) for the shear gradient vorticity normal to the interface (NV); the interface normal is along the z-direction. (b) for the shear gradient normal to the interface (NG); and (c) for the bulk (linear shear flow without interfaces). Also shown in [(c) and (d)] are the angles $\theta(\theta')$ and $\phi(\phi')$ that characterize the end-to-end vector.

1. Bead-bead steric effects are taken into account via a truncated and shifted purely repulsive Lennard-Jones potential of the form

$$U_{\mathrm{LJ}}(r)=4\epsilon\left[\left(\frac{\sigma_b}{r}\right)^{12}-\left(\frac{\sigma_b}{r}\right)^{6}-\left(\frac{\sigma_b}{r_c}\right)^{12}+\left(\frac{\sigma_b}{r_c}\right)^{6}\right], \tag{2}$$

with a cutoff at its minimum $r_c=2^{1/6}\sigma_b$. Here the bead diameter σ_b and the strength of the interaction $\epsilon=k_BT$ represent the energy and length units, respectively.

2. The "spring" is modeled via a FENE (Ref. 43) potential to ensure the connectivity between adjacent beads along the backbone, which is given by

$$U_{\mathrm{FENE}}(r)=-\frac{1}{2}KR_0^2\ln\left[1-\left(\frac{r}{R_0}\right)^2\right], \tag{3}$$

where the FENE cut-off (i.e., the allowed maximum bond length) is set to $R_0=1.5\sigma_b$ and the spring constant is $K=27\epsilon/\sigma_b^2$.[44]

3. To mimic the adsorption process, a strongly attractive interface defining the (x,y)-plane at $z=0$ is considered. Thereby, we employed a van der Waals-like attractive potential

$$U_{\mathrm{ads}}(z)=-A_0\epsilon\left(\frac{\sigma_b}{z}\right)^6 \tag{4}$$

with $A_0=5$. On top of that, a repulsive stabilizing Lennard-Jones interface potential

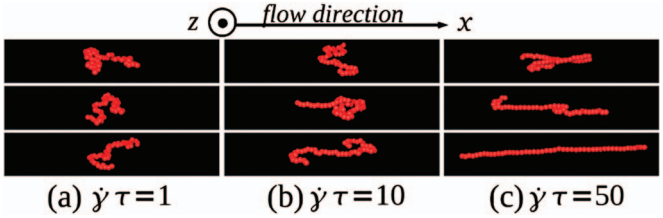

FIG. 2. Typical snapshots of polymer chains under linear shear flow in x-direction. The shear gradient direction is normal to the interface-plane (NG). Here the three columns [(a)–(c)] show configurations for three shear rates $\dot{\gamma}\tau=1$, 10, and 50.

$$U_{\mathrm{LJ}}(z)=4\epsilon\left[\left(\frac{\sigma_b}{z}\right)^{12}-\left(\frac{\sigma_b}{z}\right)^{6}-\left(\frac{\sigma_b}{z_c}\right)^{12}+\left(\frac{\sigma_b}{z_c}\right)^{6}\right], \quad (5)$$

of the same form as that in Eq. (2) (with $z_c=2^{1/6}\sigma_b$) is added, such that, the total interface potential $U_{\mathrm{interface}}(z)$ employed here is

$$U_{\mathrm{interface}}(z)=U_{\mathrm{ads}}(z)+U_{\mathrm{LJ}}(z). \quad (6)$$

A more detailed modeling for a realistic surface was used, e.g., in Ref. 45.

The BD time step is set to $\delta t=2\times10^{-6}\tau$, where $\tau=\sigma_b^2/D_0$ sets the time unit. Typically 5×10^8 BD time steps are used for data production, during which the first 5×10^7 steps are for the chain relaxation.[46] Simulation snapshots are viewed in Fig. 2.

III. RESULTS

A. Statistics of the polymer extension

We consider a single polymer chain which is advected by a shear flow and stretched by velocity inhomogeneity. The degree of the polymer stretching is characterized by the chain's end-to-end distance R_e, for which we have calculated the PDF under different shear flow geometries.

The normalized PDF of the rescaled size extension R_e/R_m, where $R_m=(N-1)R_0$ is the fully stretched chain length, is plotted in Fig. 3 for three typical selected shear rates ($\dot{\gamma}\tau=1(\square)$, $10(\diamond)$, $50(\triangle)$) for three geometries: (a) bulk, (b) NV in-plane shear gradient, and (c) NG vertical shear gradient.[47]

A general feature is that upon increasing the shear rate, chain stretching is always favored. In terms of size distribution, this shear rate induced stretching manifests itself either as a shift of the peak to larger sizes [see Figs. 3(a) and 3(b)], and/or as a thickening of the tail [see Fig. 3(c)]. The strongest stretching, at prescribed reduced shear rate $\dot{\gamma}\tau$, is obtained for the NV case. This feature can be simply explained as follows. The NV case, due to the rather strong adsorption, leads to a chain swelling (in the lateral dimensions) compared to the bulk conformations already at equilibrium (i.e., without shear flow). To elucidate this idea, we have also systematically shown the *purely two-dimensional* (2D) case (filled symbols) in Figs. 3(a) and 3(b) as a reference. Moreover, for the NV case, the shear flow deforms the polymer chain much more efficiently than in the NG case, where the

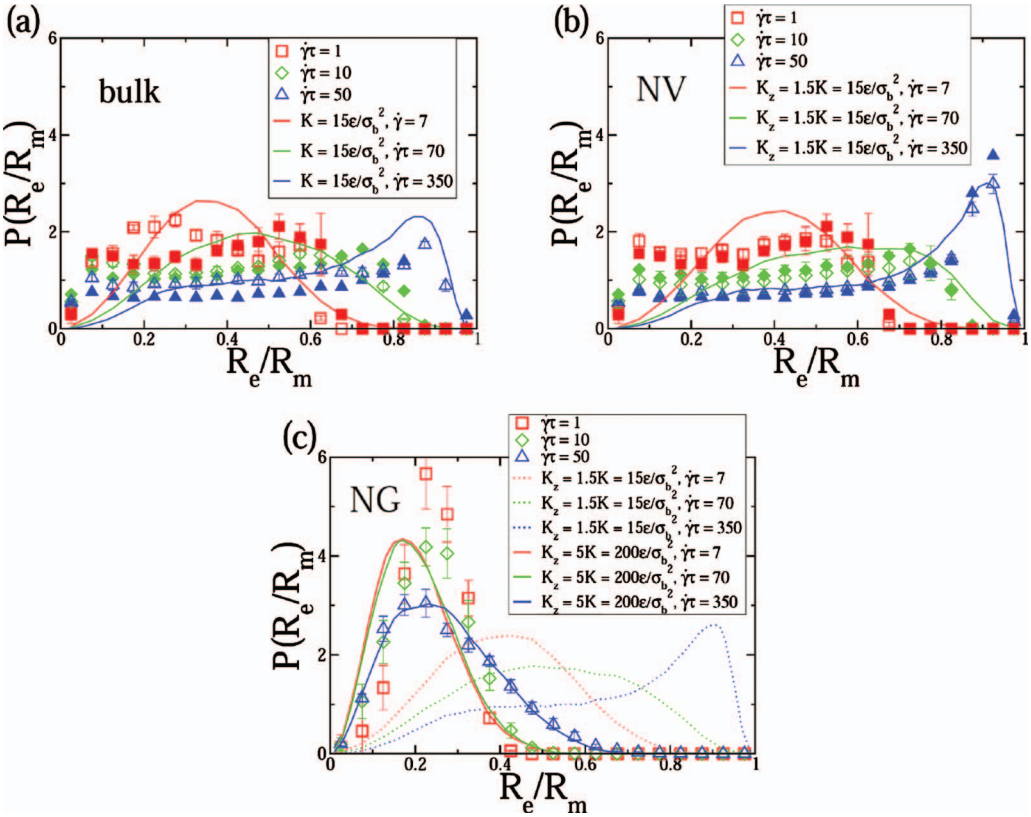

FIG. 3. The PDFs $P(R_e/R_m)$ of the reduced end-to-end distance R_e/R_m for (a) the bulk, (b) the NV case, and (c) the NG. The symbols $\square$, $\diamond$, and $\triangle$ stand for the shear rates $\dot{\gamma}\tau=1$, 10, and 50, respectively, where in [(a) and (b)], the pure 2D case is shown as a reference (filled symbols). For the FENE-dumbbell model (curves), the chosen fitting spring constant(s) parameter(s) is(are) indicated.

shear rate gradient direction is off plane. Clearly, deformations occur in the NG case because of temperature-induced fluctuations in the heights of the beads.

To broaden our understanding of the statistics of the polymer chain under shear flow, we have additionally considered the well known so-called FENE-dumbbell model.[26] The equation, describing the evolution of the end-to-end vector $\mathbf{R}_e$ of a FENE-dumbbell (i.e., a dimer), is given by

$$\mathbf{R}_e(t+\delta t) = \mathbf{R}_e(t) + \frac{D_0}{k_B T}\mathbf{F}_{\mathrm{FENE}}\delta t + \delta\mathbf{G} + \dot{\gamma}Q(t)\delta t\mathbf{e}_x, \quad (7)$$

where $\mathbf{F}_{\mathrm{FENE}}=-\nabla U_{\mathrm{FENE}}(R_e)$ is the FENE force; $\delta\mathbf{G}$ is the Gaussian term as in Eq. (1); Q is the $y-$ (or $z-$) component R_{ey} (or R_{ez}) of $\mathbf{R}_e$ assuming the shear gradient applied in the $y-$ (or $z-$) direction. To take adsorption into account in the most simple and physically sound manner within the dumbbell model, we have introduced anisotropic FENE-spring constants such that $K_x=K_y=K_z=K$ in the bulk and $[K_z > (K_x=K_y=K)]$ for NV and NG cases. The stochastic Eq. (7) was solved by using a straightforward, one-particle BD scheme integration. One has to bear in mind that this dumbbell approach is certainly relevant in the limit of strong stretching, where the degrees of freedom of "inner" monomers of a real polymer chain would be indeed heavily reduced, but cannot be suitable at low shear rates where the real chain size is dictated by the complicated distribution of the monomers.

By choosing a suitable choice of parameters [effective spring constant(s), effective shear rate] for the dumbbell model, one could always perfectly match any PDF of the full chain (results not shown). However, in order to make the comparison more physical between the dumbbell model and the full chain, we kept the spring dumbbell constant fixed as well as the ratio between the shear rates, see Fig. 3 (7:70:350=1:10:50). Given the very crude representation of the chain via a dumbbell, Figs. 3(a) and 3(b) shows a remarkable good agreement between BD data and the dumbbell model, especially at high shear rates and/or large chain size. The good agreement between these two approaches in Fig. 3(b) for the NV case also demonstrates that the idea of mimicking the adsorption with a larger dumbbell-spring constant in the z-direction is fruitful. Nonetheless, the NG case is too complex to be captured by our simple dumbbell model. Indeed, physically, the deformation in this situation is due to the z-fluctuations of the chain-beads which cannot be suitably approximated by a dumbbell. However, if we consider a stiffer (effective) dumbbell with $K_z=5K=200$ for the NG case, we can recover again a good agreement with the BD data, see Fig. 3(c).

To further characterize the statistics of the adsorbed chain under shear flow, we have calculated the first three moments of the end-to-end size distributions (the PDF in Fig. 3), which are: (i) the mean value $\langle|\mathbf{R}_e|\rangle=\langle R_e\rangle$, (ii) the variance σ^2, and (iii) the normalized third moment (so-called *skewness* S).

The mean value of the end-to-end distance is obtained as follows

$$\langle|\mathbf{R}_e|\rangle = \langle R_e\rangle = \left\langle \sum_{m=1}^{M} R_{em} \right\rangle = \frac{\Sigma_{m=1}^{M}|\mathbf{r}_{N-1}-\mathbf{r}_0|_m}{M}, \quad (8)$$

where R_{em} is the absolute value of the end-to-end vector in the mth configuration and the sum runs over the total number of the configurations M. Figure 4(a) shows that $\langle R_e\rangle$ grows with increasing $(\dot{\gamma}\tau)$, as expected. Nevertheless, in the NG case, the shear rate dependency of the end-to-end distance is relatively weak compared to the other flow geometries.

The second moment, which describes the degree of broadening about the mean value, is defined as follows:

$$\sigma^2 = \frac{\Sigma_{m=1}^{M}(R_{em}-\langle R_e\rangle)^2}{M}. \quad (9)$$

Figure 4(b) clearly shows that the variance σ^2 grows with increasing shear rate. This effect is actually due to the tumbling (more on that later) allowing the chain to cyclically stretch and recover its coil-like conformation. Thereby, the higher the shear rate the more stretched the chain can be, and consequently the larger the variance becomes. In the NG case, where stretching at prescribed shear rate is much weaker, the broadening of the size distribution is reduced accordingly.

The skewness S, a central quantity in probability theory and statistics,[48] is defined as $S=\mu_3/\sigma^3$, where μ is the third moment with respect to the mean, and σ is the standard deviation. Explicitly, the skewness was computed as follows:

$$S = \frac{\mu_3}{\sigma^3} = \frac{\frac{1}{M}\sum_{m=1}^{M}(R_{em}-\langle R_e\rangle)^3}{\left[\frac{1}{M}\sum_{m=1}^{M}(R_{em}-\langle R_e\rangle)^2\right]^{3/2}}. \quad (10)$$

It provides a quantitative and simple measure of the asymmetry of the PDF. Hence, the qualitative difference between the PDF in the NG model [see Fig. 3(c)] and those found in the other cases [see Figs. 3(a) and 3(b)] can be rationalized in terms of the value as well as the sign of S, see Fig. 4(c). For the shear gradient normal to the interface (NG), Fig. 4(c) shows that S is positive and increases with shear rate. The positivity of (S) is a signature of the statistical preponderance of the coil-sized chain configurations in the NG model. On the other hand, the skewness becomes negative and decreases (i.e., its magnitude increases) with growing shear rate in the NV model. This feature clearly indicates the preponderance of stretched chain conformations.

B. Statistics of the polymer end-to-end vector orientations

We now address the angular degrees of freedom of the end-to-end polymer chain vector, namely, ϕ and θ [depicted in Fig. 1(c)], or ϕ' and θ' [depicted in Fig. 1(d)], with respect to the prescribed shear flow x-direction as well as the shear gradient direction. Whereas ϕ/ϕ' corresponds to the usual azimuthal angle, θ/θ' is not the polar angle but rather

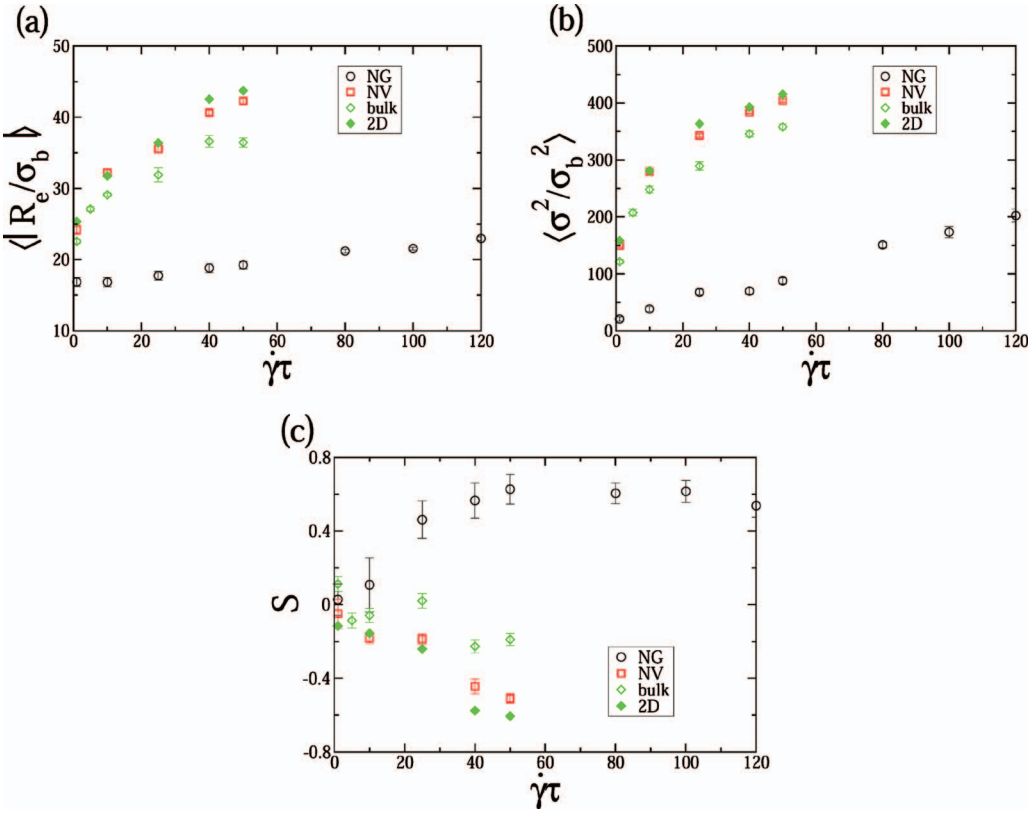

FIG. 4. The first three moments of the PDF of end-to-end distance (see Fig. 3) for the three cases (NG, NV, and bulk) plotted against the shear rate: (a) the mean value of the end-to-end distance $\langle |R_e| \rangle$; (b) the variance $\langle \sigma^2 \rangle$; and (c) the third standardized moment (S), so-called skewness. Here the solid symbols stand for the purely 2D results.

the angle formed between $\vec{R}_e$ and the plane containing the shear- and the gradient direction, see Figs. 1(c) and 1(d). Thereby we have kept the same (well established) definitions used in earlier publications.[24,49] The results for the angular distribution functions are shown in Fig. 5. As far as the azimuthal angle ϕ distribution is concerned, BD simulation data as well as the dumbbell model show a strong probability peaks in the vicinity of $\phi=0,\pi,2\pi$ in the bulk [Fig. 5(a)] and the NV case [Fig. 5(c)]. Interestingly the corresponding peak heights are not identical and, in fact, decrease with growing angles. The simple underlying physical mechanism accounting for this effect is that the torque (resulting from the shear gradient[19]) exerted on the chain favors more the conformations with $\phi \to 0$ than those with $\phi \to 2\pi$. This finding of the asymmetry in $P(\phi)$, although unexplained, was also reported in the earlier work of Celani *et al.*[26] Moreover, the larger the shear rate $\dot{\gamma}\tau$, the narrower the density probability becomes around the flow (x-axis) direction, see Figs. 5(a) and 5(c). However, the PDFs are somewhat different for the NG case, see Fig. 5(e), due to the shear gradient direction being off-plane hereby.

As far as the θ-PDFs are concerned, the shear flow induces a concentrated distribution around $\theta=0$ for all shear flow geometries, see Figs. 5(b), 5(d), and 5(f).[50] The narrowness of the peak increases again with the shear rate as expected.

In a general manner, the agreement between our simulation data and the dumbbell model (see Fig. 5) is not as satisfactory as that found for the size distribution (compare with Fig. 3). This is quite acceptable, given the crudeness of the dumbbell model. Nonetheless, the essential feature of strong depletion zones in the angular PDFs are qualitatively well captured by this dumbbell model.

The angular distribution functions were also recently studied analytically by Chertkov *et al.*[24] for a linear dumbbell in the bulk. It was thereby found to obey the following scaling law[24] $P(\phi) \sim \sin^{-2} \phi$, which was experimentally confirmed by Gerashchenko and Steinberg.[21] To establish a comparison between our simulation data and this theoretical prediction, the PDFs are plotted for a wider range of the shear rate on a linear-logarithmic plane in Fig. 6. A good agreement is found between the simulation and the scaling prediction. This is a remarkable result, since a simple harmonic dumbbell model can capture the correct scaling behavior of $P(\phi)$ of a full chain.

Concerning the θ distribution function, Chertkov *et al.*[24] have also shown a scaling behavior for the tail of the form $P(\theta) \sim \theta^{-2}$ within the framework of a linear dumbbell in the bulk. Comparison in the past with experimental results[21] demonstrated already an excellent agreement. Our results for the θ-PDF can be found in Fig. 7. The scaling prediction is again in remarkable good agreement with our BD data. Interestingly, the agreement seems to be even better for the NV case where not only the tail is dictated by θ^{-2} but the full θ-range. This suggests that the algebraic decay $P(\theta) \sim \theta^{-2}$ is even more relevant for (nearly) 2D systems.

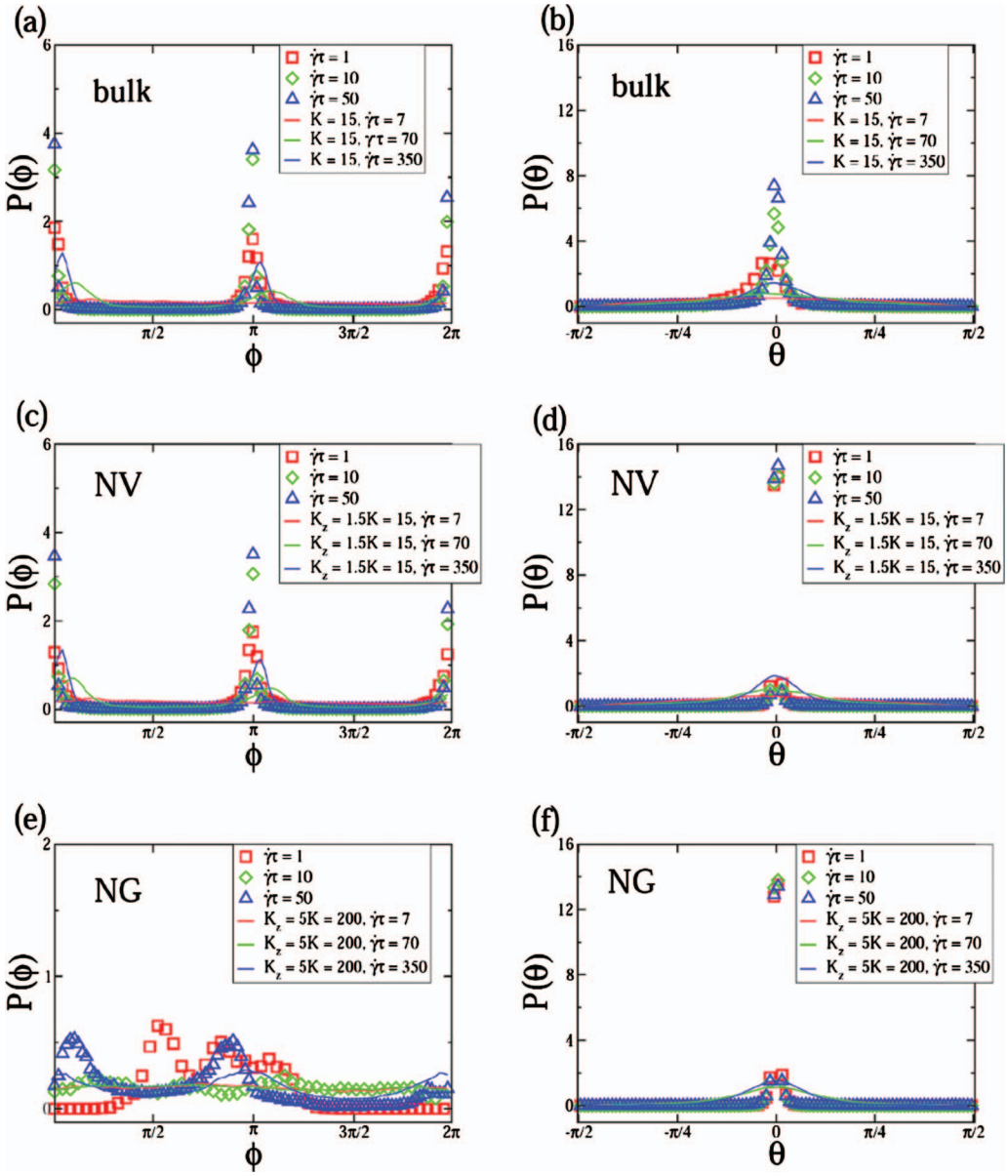

FIG. 5. The PDF of the end-to-end vector angles [see Fig. 1(c)] for the three cases (bulk, NV, and NG). The symbols and the curves stand for the same parameters as those used in Fig. 3.

C. Bond-bond angle statistics

To characterize the intrachain property under shear flow, we have considered the bond-bond angles (BBAs). This is a complementary approach to investigate the chain stretching and coiling features. The results are depicted in Fig. 8. In a first low shear rate window ($\dot{\gamma}\tau \lesssim 20$), there is a rather strong shear rate dependency for the NV, bulk, and 2D cases. Typically, this describes the relevance of coiled conformations. At higher shear rates, this dependency becomes much weaker and a plateaulike regime (about π) is observed. This feature is the signature of strongly stretched polymer chains. As far as the NG case is concerned, the shear rate dependency is much weaker as expected. This result is fully consistent with the positive skewness reported in Fig. 4(c) for a wide range of the shear rate. A complementary observable provided by the following order parameter[51] P_2 is also shown as an inset in Fig. 8

$$P_2(\cos\alpha) = \tfrac{3}{2}\left(\langle\cos^2(\pi-\alpha)\rangle - \tfrac{1}{3}\right) = \tfrac{3}{2}\left(\langle\cos^2\alpha\rangle - \tfrac{1}{3}\right). \tag{11}$$

We now would like to address the local BBAs which physically characterizes the degree of local chain stretching. The mean BBA $\langle\alpha_i\rangle$ is plotted versus the bead position index (i) in Fig. 9. As expected, a symmetry around the chain center is revealed, see Fig. 9. The two chain ends are always looser and the *local* stretching is smoothly increasing upon approaching the center of the chain. Besides, the local chain stretching increases with growing shear rate, see Fig. 9.

D. Tumbling

The tumbling process of the chain under shear flow is the mechanism by which energy is transferring, or in other words, the polymer cyclically absorbs (stretching) and releases (collapsing) energy from and to the surrounding fluid.

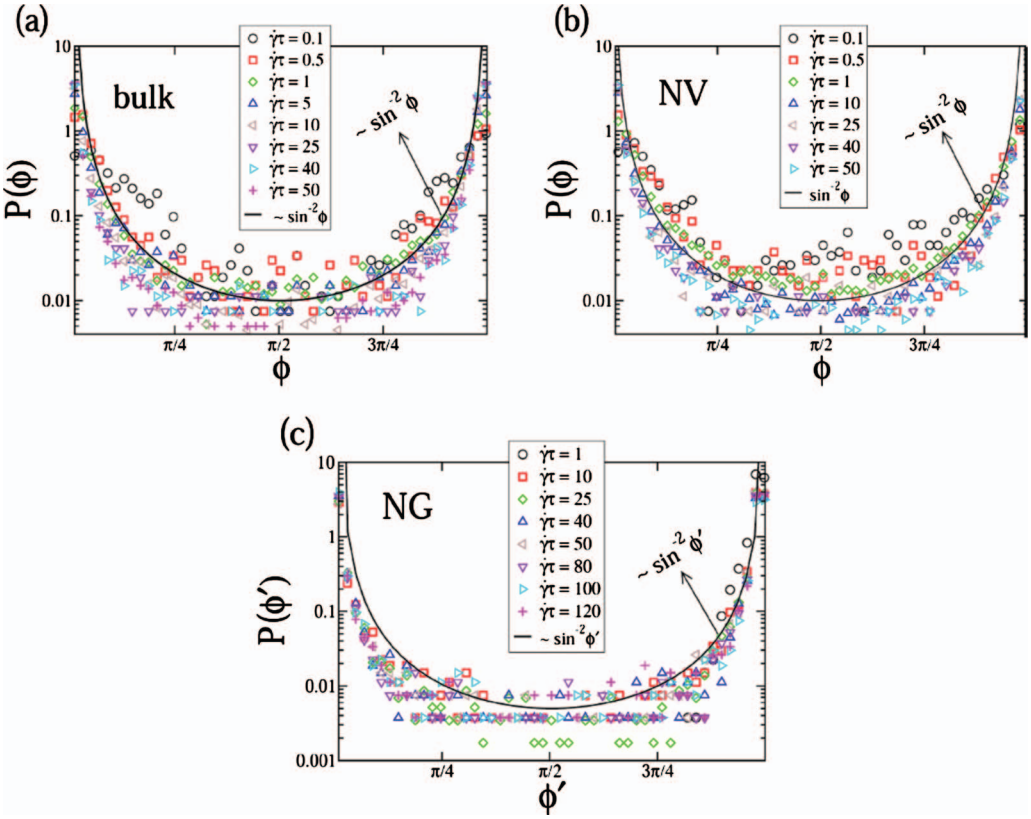

FIG. 6. The PDF of the in-shear-gradient-plane angle $\phi(\phi')$ [sketched in Figs. 1(c) and 1(d)]. The solid curves are the theoretical scaling predictions ($\sim \sin^{-2}\phi$ or $\sin^{-2}\phi'$) of the dumbbell model (Refs. 24 and 27).

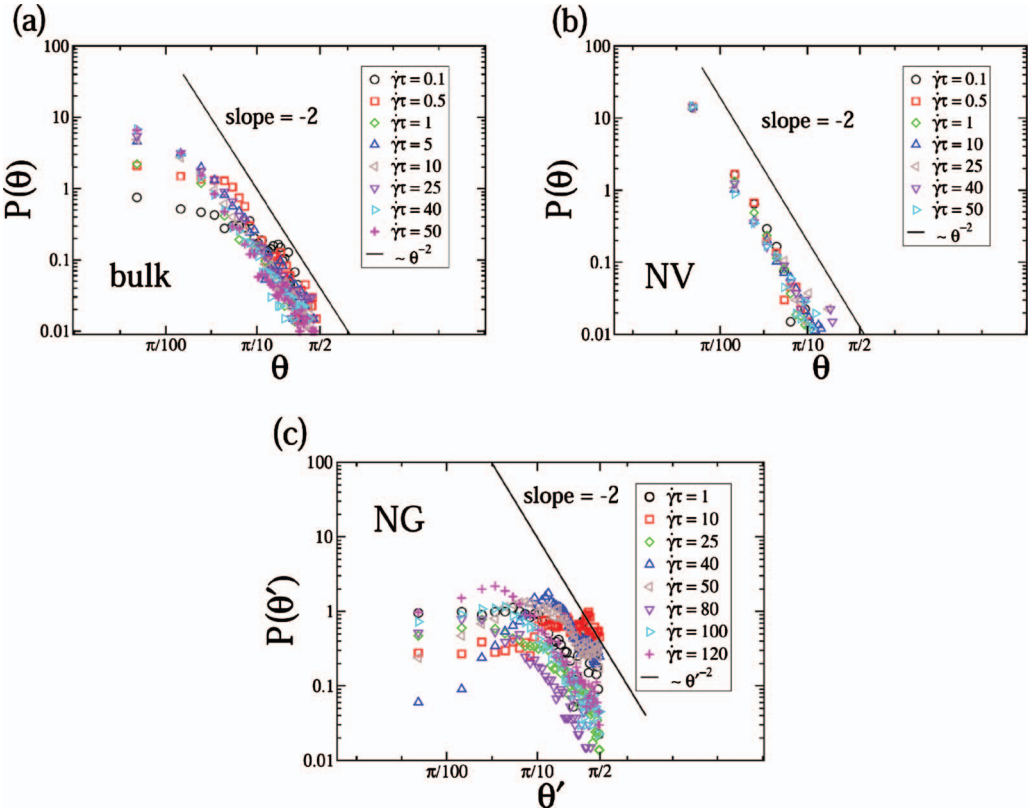

FIG. 7. The PDF of the off-shear-gradient-plane angle $\theta(\theta')$ [sketched in Figs. 1(c) and 1(d)]. The solid curves are the theoretical scaling predictions ($\sim \theta^{-2}$ or θ'^{-2}) of the dumbbell model (Refs. 24 and 27).

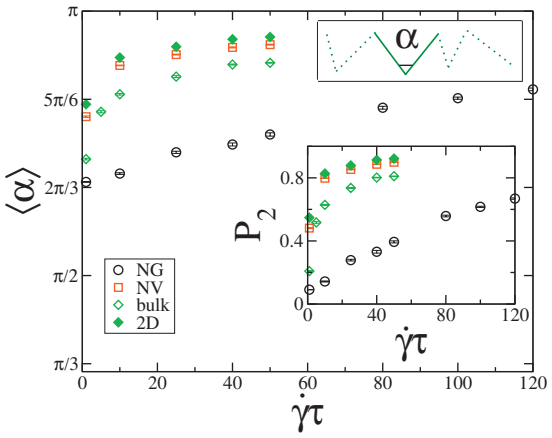

FIG. 8. The average BBA $\langle\alpha\rangle$ plotted against the reduced shear rate $\dot{\gamma}\tau$. Inset: the order parameter $P_2(\cos\alpha)$.

This particular polymer motion in-shear flow has been thoroughly studied in the past.[19,20,35] All these studies address the bulk case[19,20] or grafted polymer chains,[35] but without considering the problem of adsorption. In this work, the frequency of this cyclic motion is calculated for the three geometries (bulk, NV, and NG) via the Fourier transform of the time-dependent radius of gyration, which is

$$R_g(t) = \sqrt{\frac{\Sigma_{i=0}^{N-1}(\mathbf{r}_i(t) - \mathbf{r}_{\mathrm{cm}}(t))^2}{N}}, \tag{12}$$

where $\mathbf{r}_{\mathrm{cm}}(t) = \Sigma_{i=0}^{N-1}\mathbf{r}_i(t)/N$ is the chain center of mass at time t. The first main peak position of the resulting Fourier transform of $R_g(t)$ (not shown here) is chosen as the tumbling frequency.

Figure 10 displays the reduced tumbling frequency ($\nu\tau$) as a function of the reduced shear rate $\dot{\gamma}\tau$. The purely 2D case is also shown as a reference. Thereby, scaling behaviors of the form

$$\nu\tau \sim (\dot{\gamma}\tau)^{\lambda},$$

are observed with $\lambda = 0.90, 0.71, 0.72$ for NG, NV, and bulk, respectively. Hence, the bulk and NV cases exhibit (within statistical uncertainties) an identical scaling behavior for the tumbling frequency. The value found for the exponent $\lambda \approx 0.7$ is in very good agreement with the one reported by Schroeder *et al.*[19] ($\lambda = 0.67$), based on the angular power spectral frequency, for Brownian rods in the bulk. As expected the NG case exhibits a different scaling behavior (here $\lambda = 0.9$) due to the chain adsorption that weakens the effect of the velocity gradient in the normal direction.

To understand the physical origin of the observed scaling behavior of the tumbling frequency in Fig. 10, we are going to employ the arguments advocated by Teixeira *et al.*[20] By decomposing the tumbling motion into typical time periods: (i) a stretching phase (t_{stretch}), (ii) an alignment along the shear direction (t_{align}), (iii) a flip motion (t_{flip}), and (iv) a collapse event (t_{collapse}), we can write an expression for the tumbling frequency[19,20] ν

$$\nu\tau \propto \frac{\tau}{t_{\mathrm{stretch}} + t_{\mathrm{align}} + t_{\mathrm{flip}} + t_{\mathrm{collapse}}}. \tag{13}$$

The three processes of polymer stretching, aligning, and collapsing being advection-driven, Teixeira *et al.*[20] have shown that t_{stretch}, t_{align}, and t_{collapse} scale like $\langle X\rangle/(\dot{\gamma}\tau)\langle\delta_2\rangle$, where $\langle X\rangle$ is the average chain extension in the x-flow direction and

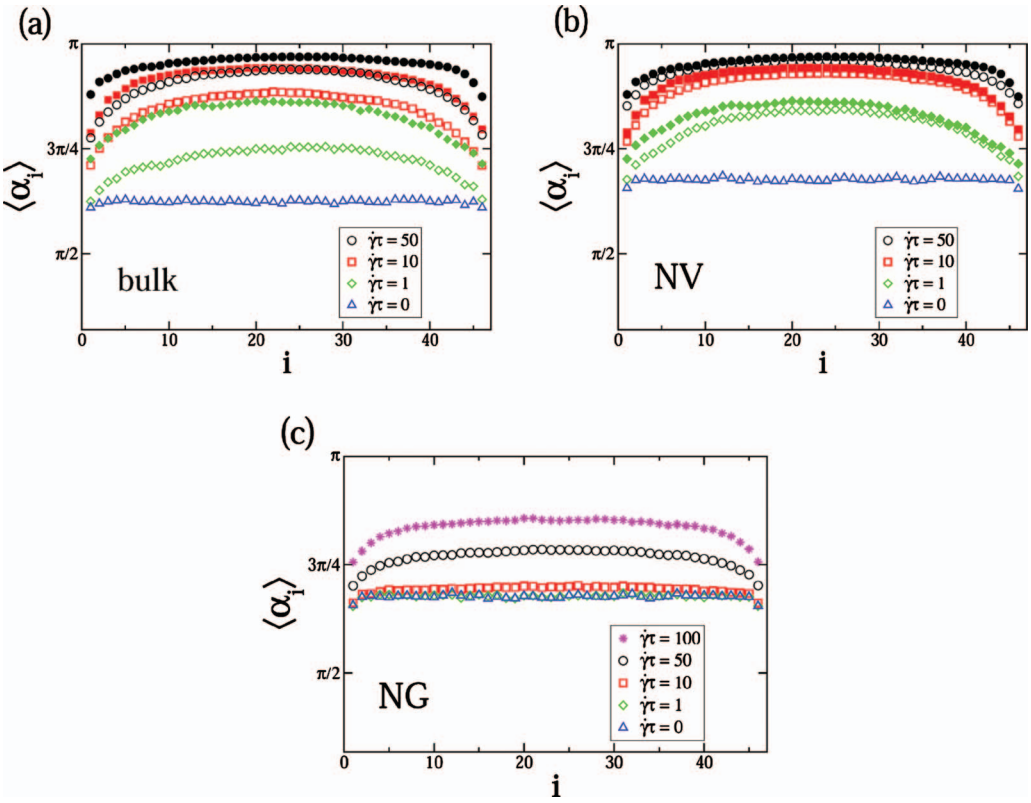

FIG. 9. The mean local BBA $\langle\alpha_i\rangle$ of bead (i). The solid symbols in [(a) and (b)] represent the purely 2D case.

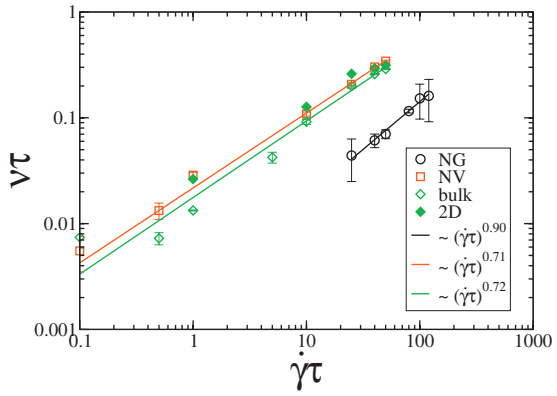

FIG. 10. Reduced tumbling frequency $\nu\tau$ as a function of the reduced shear rate $\dot{\gamma}\tau$. The lines correspond to the best fit.

$\langle\delta_2\rangle$ is the chain extension in the shear gradient direction. On the other hand, the flipping process is a diffusive motion such that $t_{\text{flip}} \sim \langle\delta_2\rangle^2 / D(\delta_2) \sim \langle\delta_2\rangle^{8/3}$,[20] where $D(\delta_2)$ is the diffusivity in the shear gradient direction and found to be $D(\delta_2) \sim \delta_2^{-2/3}$ from BD simulations by Doyle *et al.*[52] Following the same procedure with our simulation data, we were then able to extract the time duration scalings which are gathered in Table I.

These results in Table I are in good agreement, for the NV case and the bulk, with the observed exponent ($\lambda = 0.7$, see Fig. 10). Even for the NG case, the scaling predictions are validated for the convective processes (stretching, alignment, and collapsing). Nonetheless, it fails for t_{flip} in the NG case because the strong adsorption weakens the diffusivity in the shear gradient ($z-$) direction $D(\delta_2)$.

IV. CONCLUSION

Using BD simulations, the statistical properties of adsorbed polymers under a linear shear flow have been studied for the two cases: in-adsorption-plane shear gradient (or equivalently the shear vorticity normal to the adsorbing interface) and the shear gradient perpendicular to the interface. The three-dimensional bulk and the purely 2D cases under linear shear flow have been considered as well as reference cases.

We have compared the behavior of the full polymer chain to that of a simple dumbbell model. A good agreement is reached for the PDF of the chain end-to-end distance. Besides, the theoretically predicted scaling behavior[24,27] of the angular PDF tails is confirmed also in the case where the shear gradient is parallel to the interfaces (NV case). In the opposite case of perpendicular shear gradient (NG case), agreement is only found at high shear rates. It is remarkable that a simple dumbbell model can capture the correct scaling behavior of the angular PDFs' tails of a full chain.

TABLE I. Characteristic times involved in the tumbling motion discussed in the text.

	t_{stretch}	t_{align}	t_{collapse}	t_{flip}
Bulk	$\sim(\dot{\gamma}\tau)^{-0.62}$	$\sim(\dot{\gamma}\tau)^{-0.62}$	$\sim(\dot{\gamma}\tau)^{-0.62}$	$\sim(\dot{\gamma}\tau)^{-0.67}$
NV	$\sim(\dot{\gamma}\tau)^{-0.64}$	$\sim(\dot{\gamma}\tau)^{-0.64}$	$\sim(\dot{\gamma}\tau)^{-0.64}$	$\sim(\dot{\gamma}\tau)^{-0.61}$
NG	$\sim(\dot{\gamma}\tau)^{-0.87}$	$\sim(\dot{\gamma}\tau)^{-0.87}$	$\sim(\dot{\gamma}\tau)^{-0.87}$	$\sim(\dot{\gamma}\tau)^{0.40}$

The chain coiling and stretching degree was characterized by the inner bond-bond angles. For the NV, bulk, and 2D cases, the shear rate dependency is found to be rather strong in the first low shear rate regime, but is much weaker at higher shear rates, and a plateaulike behavior is approached once the shear rate is high enough. For the NG case, this dependency is much weaker for a wide range of shear rates.

The tumbling frequency in the bulk scales sublinearly with shear flow rate which is in agreement with the early studies.[19,20] We found this sublinear scaling also in the adsorbed cases (NV and NG). The theoretical scaling analysis based on the dumbbell model[20] was confirmed for the NV case but not for the NG case.

As an outlook, understanding the stretching and coiling mechanisms of polymer in flow leads to an improved control over chain configurations in various circumstances of confinement, e.g., in microfluidic devices.[4] Stretched polymer chains may provide valuable candidates for nanowires in microcircuits.[6] Therefore a minimalistic model, as the simple FENE-dumbbell model, is useful in order to map the behavior of a complex system and to predict the qualitative trends in various flow situations.

For future studies, many polymer chains, i.e., a concentrated polymer solution, may exhibit complex dynamical behavior due to significant slowing down caused by mutual chain entanglements.[53] It is further interesting to mix nanoparticles and polymers[54] and expose them to different flow fields and study their collective dynamical behavior.[55] Finally, the influence of HIs need further consideration, since at a high enough shear rate, polymer chains should desorb due to the bead-wall HI.[56]

ACKNOWLEDGMENTS

We thank A. Kiriy and M. Stamm for helpful discussions. This work was supported by the DFG (Grant Nos. LO 418/12-1 and SFB TR6).

[1] B. D. Ratner and S. J. Bryant, Annu. Rev. Biomed. Eng. **6**, 41 (2004).
[2] P. L. Felgner, Sci. Am. **276**, 102 (1997).
[3] F. Rusmini, Z. Y. Zhong, and J. Feijen, Biomacromolecules **8**, 1775 (2007).
[4] S. Köster, D. Steinhauser, and T. Pfohl, J. Phys. Condens. Matter **17**, S4091 (2005).
[5] E. Braun, Y. Eichen, U. Sivan, and G. Ben-Yoseph, Nature (London) **391**, 775 (1998).
[6] A. Knobloch, A. Manuelli, A. Bernds, and W. Clemens, J. Appl. Phys. **96**, 2286 (2004).
[7] T. Kotaka, H. Suzuki, and H. Inagaki, J. Chem. Phys. **45**, 2770 (1966).
[8] J. D. Huppler, E. Ashare, and L. A. Holmes, Trans. Soc. Rheol. **11**, 159 (1967).
[9] C. Tiu, T. Moussa, and R. J. Carreau, Rheol. Acta **34**, 586 (1995).
[10] J. Marko and E. D. Siggia, Macromolecules **28**, 8759 (1995).
[11] C. Rivetti, M. Guthold, and C. Bustamante, J. Mol. Biol. **264**, 919 (1996).
[12] D. E. Smith, H. P. Babcock, and S. Chu, Science **283**, 1724 (1999).
[13] B. Ladoux and P. S. Doyle, Europhys. Lett. **52**, 511 (2000).
[14] S. Minko, A. Kiriy, G. Gorodyska, and M. Stamm, J. Am. Chem. Soc. **124**, 3218 (2002).
[15] L. J. Kirwan, G. Papastavrou, M. Borkovec, and S. H. Behrens, Nano Lett. **4**, 149 (2004).

[16] E. S. G. Shaqfeh, J. Non-Newtonian Fluid Mech. **130**, 1 (2005).
[17] S. W. Schneider, S. Nuschele, A. Wixforth, C. Gorzelanny, A. Alexander-Katz, R. R. Netz, and M. F. Schneider, Proc. Natl. Acad. Sci. U.S.A. **104**, 7899 (2007).
[18] G.-L. He, R. Messina, H. Löwen, A. Kiriy, V. Bocharova, and M. Stamm, Soft Matter **5**, 3014 (2009).
[19] C. M. Schroeder, R. E. Teixeira, E. S. G. Shaqfeh, and S. Chu, Phys. Rev. Lett. **95**, 018301 (2005).
[20] R. E. Teixeira, H. P. Babcock, E. S. G. Shaqfeh, and S. Chu, Macromolecules **38**, 581 (2005).
[21] S. Gerashchenko and V. Steinberg, Phys. Rev. Lett. **96**, 038304 (2006).
[22] E. J. Hinch, J. Fluid Mech. **74**, 317 (1976).
[23] E. J. Hinch, J. Fluid Mech. **75**, 765 (1976).
[24] M. Chertkov, I. Kolokolov, V. Lebedev, and K. Turitsyn, J. Fluid Mech. **531**, 251 (2005).
[25] R. G. Winkler, Phys. Rev. Lett. **97**, 128301 (2006).
[26] A. Celani, A. Puliafito, and K. Turitsyn, Europhys. Lett. **70**, 464 (2005).
[27] A. Puliafito and K. Turitsyn, Physica D **211**, 9 (2005).
[28] M. Chopra and R. G. Larson, J. Rheol. **46**, 831 (2002).
[29] A. S. Panwar and S. Kumar, J. Chem. Phys. **122**, 154902 (2005).
[30] N. Hoda and S. Kumar, J. Rheol. **51**, 799 (2007).
[31] N. Hoda and S. Kumar, J. Chem. Phys. **127**, 234902 (2007).
[32] N. Hoda and S. Kumar, J. Chem. Phys. **128**, 164907 (2008).
[33] C. Aust, S. Hess, and M. Kröger, Macromolecules **35**, 8621 (2002).
[34] S. Liu, B. Ashok, and M. Muthukumar, Polymer **45**, 1383 (2004).
[35] R. Delgado-Buscalioni, Phys. Rev. Lett. **96**, 088303 (2006).
[36] M. Müller and C. Pastorino, Europhys. Lett. **81**, 28002 (2008).
[37] L. Cannavacciuolo, R. G. Winkler, and G. Gompper, Europhys. Lett. **83**, 34007 (2008).
[38] A. Serr and R. R. Netz, Europhys. Lett. **78**, 68006 (2007).
[39] P. S. Doyle, E. S. G. Shaqfeh, and A. P. Gast, Macromolecules **31**, 5474 (1998).
[40] I. M. Neelov and K. Binder, Macromol. Theory Simul. **4**, 119 (1995).
[41] The NG case is possibly at least partially realized in spin coating processes. The kinematics of spin coating are actually rather complex [see, e.g., D. E. Bornside, C. W. Macosko and L. E. Scriven, J. Appl. Phys. **66**, 5185 (1989)]. (There is indeed a flow in the "tangential direction," which is modeled by the NG case. However, there is also film thinning, which will give the velocity field an extensional component. The film thinning process will tend to drive chains toward the substrate. Polymer-wall HI will tend to push chains away from the substrate. So, it is possible that these two effects cancel each other.)
[42] Indeed for a solid wall and incompressible fluid (i.e., $\nabla \cdot \mathbf{v}=0$ with $\mathbf{v}$ being velocity field), the velocity field $\mathbf{v}$ is conserved at the solid-liquid interface. Typically, if the substrate is at rest, $\mathbf{v}$ must vanish at the boundary. See E. Guyon, J. P. Hulin, L. Petit, and C. D. Mitescu, *Physical Hydrodynamics* (Oxford University Press, New York, 2001).
[43] K. Kremer and G. S. Grest, J. Chem. Phys. **92**, 5057 (1990).
[44] It is to say that in our model, we implicitly assume that the spring laws, stemming from the bulk conditions, remain unchanged close to the interface. Thereby the possible anisotropy mediated in the vicinity of the interface is neglected. This feature was addressed in the work by N. J. Woo, E. S. G. Shaqfeh, and B. Khomami, J. Rheol. **48**, 281 (2004); N. J. Woo, E. S. G. Shaqfeh, and B. Khomami, *ibid.* **48**, 299 (2004).
[45] D. Andrienko, S. Leon, L. D. Site, and K. Kremer, Macromolecules **38**, 5810 (2005).
[46] Given the strong adsorption, the NG case (normal shear gradient) requires more computational time for good statistics, so that even 10^9 BD steps were used.
[47] In the figures of the results section, all the error bars were calculated using five (for the bulk case) and ten (for NV and NG) independent simulation runs.
[48] D. N. Joanes and C. A. Gill, J. R. Stat. Soc. **47**, 183 (1998).
[49] E. J. Hinch and L. G. Leal, J. Fluid Mech. **52**, 683 (1972).
[50] Note that the symmetry of the shear flow imposes a symmetry of $P(\theta)$ about $\theta=0$.
[51] G.-L. He, H. Merlitz, J.-U. Sommer, and C.-X. Wu, Macromolecules **40**, 6721 (2007).
[52] P. S. Doyle, E. S. G. Shaqfeh, and A. P. Gast, J. Fluid Mech. **334**, 251 (1997).
[53] F. Varnik and K. Binder, J. Chem. Phys. **117**, 6336 (2002).
[54] A. Jusufi, J. Dzubiella, C. N. Likos, C. von Ferber, and H. Löwen, J. Phys. Condens. Matter **13**, 6177 (2001).
[55] O. B. Usta, D. Perchak, A. Clarke, J. M. Yeomans, and A. C. Balazs, J. Chem. Phys. **130**, 234905 (2009).
[56] In Hoda and Kumar's work (Ref. 31), polyelectrolytes are treated. It is found that at strong screening, the depletion layer thickness L_d scales as $L_d \sim W_i^{2/3}$ (W_i being the Weissenberg number) at high W_i. (See Fig. 11 in Ref. 31.) Although this finding concerns polyelectrolytes, it should also be relevant for neutral polymers as it is the case in our study.